ADVANCED FUNCTIONAL MATERIALS
www.afm-journal.de

Unraveling the Missing Link of Bio-Electrical Stimulation from Body-Mediated Energy Transfer

Sungwon Jung, Hyungseok Yong, Milae Lee, Banseok Kim, Tae-Yun Kang, Hun Soo Jang, Woo Jin Choi, Dongchang Kim, Moonhyun Choi, Geul Bang, Heeyoun Hwang, Sung-Hwan Choi, Jinkee Hong,* and Sangmin Lee**

As the technologies for treating diseases are attracting continuous attention, physical therapy methods, particularly electrical stimulation (ES), have been widely investigated owing to their high effectiveness. As ES essentially requires an external power source, various efforts are being devoted to achieving the application of ES to the human body using nanogenerators. Various studies have verified the effect of ES by applying the same output generated by the device to in vitro and in vivo bio-electrical stimulation. However, it is unknown whether the electrical output generated by the device can be transmitted equally in the cell unit, and this is considered a common missing link in bio-electrical stimulation research. Herein, the missing link between electrical devices and in vitro bio-electrical stimulations is unraveled by the ex vivo, 2D simulation, and in vitro study of body-mediated energy transfer (BmET) models. In addition, BmET-based ES is applied to pre-osteoblasts, and the increased cellular functions are verified.

1. Introduction

Physical therapy has attracted attention because of its low side effects and higher effectiveness.[1] Among various physical therapy methods, electrical stimulation (ES) has attracted research attention for the management and treatment of body dysfunction and disease.[2] The effect of ES on the human body is exerted from the cellular level, and it promotes healing or recovery from disease through the activation of cellular functions.[3] Briefly, the ES of cells induces a change in the cell membrane potential, which spontaneously depolarizes the voltage-gated ion channels (VGICs) in the cell membrane, and activates the mitochondria.[4] These cellular activations by ES can promote the production of adenosine triphosphate (ATP) or increase the ion acceptance of the individual cell, thus increasing cell proliferation and differentiation.[2b] However, as ES inevitably requires an extra energy source or wires, there are limitations to its application in daily life. To overcome these limitations, various energy harvesting methods based on the use of the motions of the human body or the surrounding

S. Jung, H. Yong, M. Lee, J. Hong
Department of Chemical & Biomolecular Engineering
College of Engineering
Yonsei University
50 Yonsei-ro, Seodaemun-gu, Seoul 03722, Republic of Korea
E-mail: jinkee.hong@yonsei.ac.kr

H. Yong, B. Kim, D. Kim, S. Lee
School of Mechanical Engineering
Chung-ang University
84, Heukseok-ro, Dongjak-gu, Seoul 06974, Republic of Korea
E-mail: slee98@cau.ac.kr

H. Yong, H. S. Jang, W. J. Choi
Chemical Materials Solutions Center
Korea Research Institute of Chemical Technology (KRICT)
141 Gajeong-ro, Yuseong-gu, Daejeon 34114, Republic of Korea

T.-Y. Kang
Department and Research Institute of Dental Biomaterials and Bioengineering
Yonsei University College of Dentistry
50–1 Yonsei-ro, Seodaemun-gu, Seoul 03722, Republic of Korea

H. S. Jang
Materials Digitalization Center
Korea Institute of Ceramic Engineering & Technology (KICET)
101 Soho-ro, Jinju-si 52851, Republic of Korea

M. Choi
Center for Systems Biology
Massachusetts General Hospital
Boston, MA 02114, USA

G. Bang, H. Hwang
Research Center for Convergence Analysis
Korea Basic Science Institute
Cheongju 29118, Republic of Korea

H. Hwang
Critical Diseases Diagnostics Convergence Research Center
Korea Research Institute of Bioscience and Biotechnology
Daejeon 34141, Republic of Korea

S.-H. Choi
Department of Orthodontics
Institute of Craniofacial Deformity
Yonsei University College of Dentistry
50–1 Yonsei-ro, Seodaemun-gu, Seoul 03722, Republic of Korea
E-mail: selfexam@yuhs.ac

The ORCID identification number(s) for the author(s) of this article can be found under https://doi.org/10.1002/adfm.202302465

DOI: 10.1002/adfm.202302465

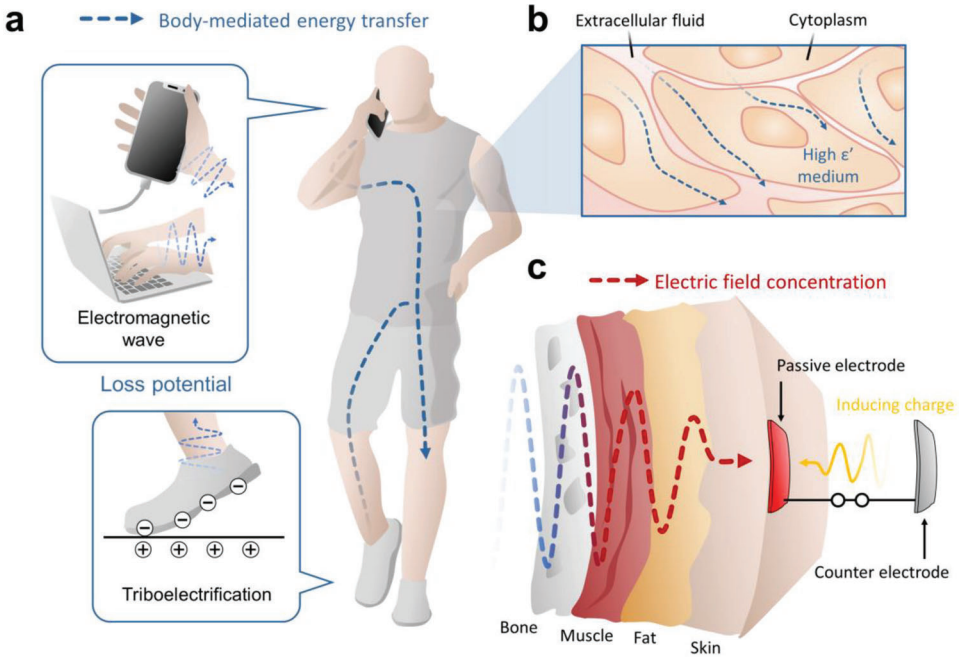

Scheme 1. Mechanism of body-mediated energy transfer (BmET)-based electrical stimulation (ES). a) Loss potentials from electronics (electromagnetic waves) and physical activities (triboelectrification). b) Potential transfer via high relative permittivity medium in the human body (cytoplasm, extracellular fluid). c) Electric field concentration via charge inducing when loss potential is transmitted through biological tissues.

environment, such as triboelectric and piezoelectric nanogenerators, have been reported for the application of ES to the body without an external power source.[5] Nevertheless, these investigated methods can cause user discomforts, such as requiring a large area device or wire connection between a target area and the energy harvesters.

Recently, to overcome these issues, a self-powered and wireless body-mediated energy transfer (BmET)-based ES system,[2a,b,6] which involves the transmission of electric potential in the form of electromagnetic waves through the human body,[7] has been developed. Particularly, non-sinusoidal potential generated by repeated physical activity (walking, touching) via triboelectrification, including sinusoidal potential generated by electronic devices (e.g., laptop and cell phone), can be transmitted through the human body (**Scheme 1**a).[8] As biological tissues (consisting of cytoplasm and extracellular fluid) with high permittivity do not cause dielectric loss at electric fields below 1 kHz,[9] a low-frequency potential (loss potential) from electronics and triboelectrification of physical activity can be transferred regardless of distance (Scheme 1b).[8] When the loss potential is transferred to a passive electrode attached to the human body, which is connected to a counter electrode, potential distortion occurs owing to an induced charge between the electrodes (Scheme 1c).[6] Consequently, BmET-based ES forms a local electric field concentration in biological tissues (e.g., skin, fat, muscle, and bone) near the passive electrode, resulting in positive physiological effects (e.g., wound healing[2b] and hair regeneration[2a]). Previously reported nanogenerators-based ES systems, including the BmET, apply electrical output from energy harvesters to bio-electrical stimulation setup (from in vitro to in vivo) to verify the activation of cell functions, such as cell proliferation, migration, and differentiation. However, interrelationships, such as whether the electric field applied to in vitro and in vivo setups is the same as the electric field measured in clinical and ex vivo setups, have not yet been identified. In addition, how this electric field affects biological tissues (e.g., fat, muscle, and bone) under the skin has not been confirmed. These steps can be considered as the "missing links" between the output from the device for the bio-electrical stimulation.

Here, we identified the interrelationships between preclinical tests and BmET-based ES devices. The similarity between the actual experimental results and the finite element analysis (FEA)-calculated results of the BmET-based ES based on an ex vivo setup was verified. The results of the 2D multi-physical simulation models were perfectly matched with those of the ex vivo model, and both models exhibited similar electrical outputs and waveforms. As a model cell of pre-osteoblasts, which are deposited in the bone model, 2D axisymmetric simulation models based on the in vitro experimental setup were constructed and the electrical input was adjusted to match the electric field formed in the ex vivo setup. Subsequently, based on the calculated input data, the activation of cellular function when the corresponding electrical output was applied to the pre-osteoblast cells was investigated. Lastly, the increased proliferation and differentiation of pre-osteoblasts by the BmET-based ES was verified without any missing links between the in vitro bio-electrical stimulation model and ex vivo electrical devices.

2. Results and Discussion

2.1. Electrical Stimulation via Body-Mediated Energy Transfer in Daily Life

All low-frequency electric fields from electronic devices and physical activities inevitably exposed in daily life, including artificially induced input sources such as nanogenerators, can be

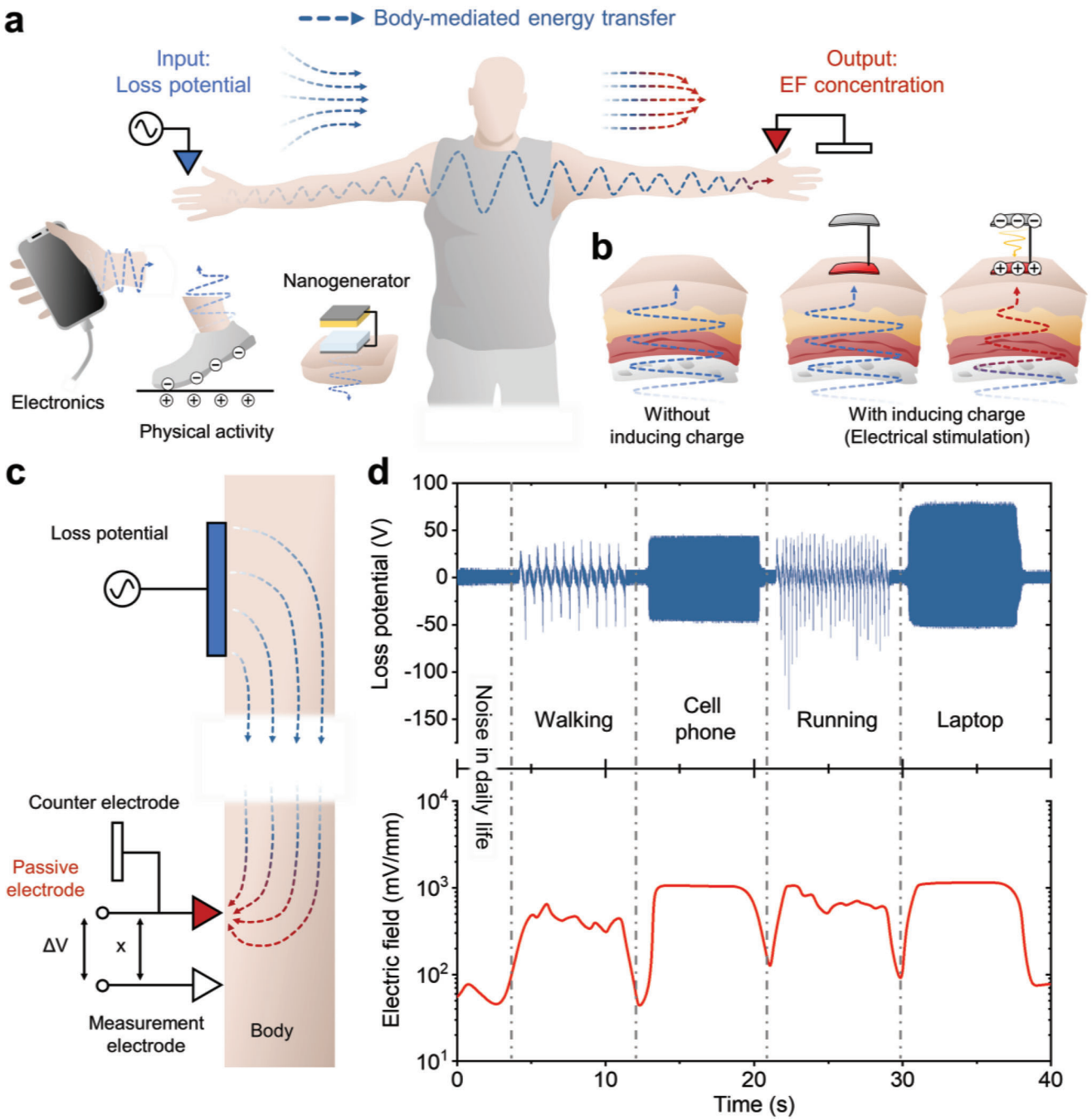

Figure 1. ES based on BmET in daily life. a) Loss potentials from electronic devices, physical activity, nanogenerators, etc. are transmitted through the human body. b) Without inducing charge, transferred energy is radiated on the skin. With inducing charge, local electric field concentration occurs (electrical stimulation). c) Measurement setup of electric field strength. d) Loss potentials and electric field concentration in daily life.

transmitted through the human body (**Figure 1**a). Typically, these input sources enter the human body through a large area, so the electric flux density is low. In general cases, the transmitted energy is radiated and dissipated through the other skin (Figure 1b). However, if there are passive electrodes on the human body connected to the corresponding counter electrode, induced charges flow between the electrodes, establishing electrical equilibrium. Sudden changes in the potential difference between the passive electrode and skin increase the electric field strength, leading to the formation of localized electric field concentrations (electrical stimulation). The intensity of this electric field can be easily measured using a non-grounded multimeter (Figure 1c,d, detailed in experimental section). A simple passive electrode and counter electrode setup was implemented, where the passive electrode is a stripped wire with a diameter of 0.25 mm and a length of 1 cm, and the measurement electrode of the same size was used. The

counter electrode was earth-grounded for stable measurements. When the passive electrode is present, weak electric fields are formed beneath it due to exposure to electrical noise in daily life (e.g., buried cable, electronics, etc.). As a human begins to walk or run, non-sinusoidal loss potentials occur due to triboelectrification generated between the shoes and the floor. This leads to the formation of irregular electric fields beneath the passive electrode. When the human grips or touches electronics, a stable electric field is formed beneath the passive electrode because the electronic device has a sinusoidal loss potential (60 Hz). These results suggest that effective non-powered and wireless electrical stimulation can be implemented in daily life through the implementation of very simple passive electrodes and counter electrodes.

2.2. 2D Simulation of the Ex Vivo Model

To measure the electric field induced by the BmET-based ES in biological tissues, including bones, pork front feet were utilized as an ex vivo model for BmET-based ES (**Figure 2**a).[2b,6] In addition, the ex vivo model was converted to 2D multi-physical simulation models (electrostatic and electrical circuit), which was laminated from the inside into bone, muscle, fat, and skin (Figure 2b). A passive electrode was attached to the skin at a boundary corresponding to a circumference of 5 degrees, and a counter electrode was placed vertically away from the passive electrode to avoid interference (Figure S1a, Supporting Information). The loss potential was applied to the skin located on the opposite side of the passive electrode (a circumference of 60 degrees). The two electrodes implemented as floating ground were connected at a circuit resistance of 10 Ω, and earth ground was connected to the counter electrode (Figure S1b, Supporting Information). The relative permittivity of the bone, muscle, fat, and skin was set as 8.3×10^3, 2.6×10^7, 8.9×10^6, and 1.1×10^5, respectively.[9a] The output generated by the actual loss potential generators was measured, and the non-sinusoidal (6 Hz, physical activity) and sinusoidal loss (60 Hz, electronics) potentials simulating the waveform of the actual loss potentials were applied to the bottom skin (Figure 2c,d). When the loss potential (input) was transferred through the biological tissues, charges were induced between the passive and counter electrodes, and the electric field (output) was concentrated under the passive electrode owing to the distortion in the electrical potential, as expressed in the following equation (Figure 2e).

$$E = -\nabla V \tag{1}$$

The output values were measured at the centers of the skin, fat, and muscle, and on the surface of the bone (Figure 2f). In the case of the non-sinusoidal loss potential, the potential decreased rapidly, as the distance approached the passive electrode (Figure 2g). This indicates that the connection between the passive and counter electrodes induced charges to maintain a state of electrical equilibrium in real-time by the transmitted potential, thus causing potential distortion. In the case of the sinusoidal loss potential generated in the electronic devices, the same aspect of potential distortion was exhibited because there was no dielectric loss owing to a low frequency (Figure 2h). As the intensity of the electric field was determined according to the magnitude of potential distortion, each tissue exhibited different intensities (Figure 2i–k). The largest electric field was formed on the skin, which was closest to the passive electrode, and the smallest electric field was formed in the muscles, which was farthest from the passive electrode and with a high permittivity.

The extreme difference in the intensity of the electric field of the tissue could be attributed to the fact that the permittivity ratio was higher than powers of 10 (10^3–10^7). However, as real biological tissue is not divided into steps but is intricately intertwined, it is necessary to increase the accuracy of the simulation by imitating real biological tissue models. To imitate actual tissues, the permittivity between each tissue was smoothed to change linearly (**Figure 3**a). When only the outside of the bone was smoothed (Smoothed, $*\epsilon_r$), the average permittivity of the tissues except the bone increased, whereas the potential in the bone decreased rapidly (Figure 3b). This indicates that a larger electric field was formed inside the bone (Figure 3c). However, if the entire bone was smoothed (Extremely smoothed, $**\epsilon_r$), the transmission aspect of the potential becomes similar to that of the step ϵ_r. Detailed results of transferred potential and electric field according to the revised permittivity model are demonstrated in Figures S2–S7, Supporting Information. In fact, the measured experimental results revealed that the strength of the electric field decreased from the skin, and then increased slightly between the muscle and the bone. This indicates that the electric field was strongly applied to the outside of the bone because the permittivity of the bone was relatively smaller than those of other tissues, which was also confirmed in all simulation cases. The results obtained under extremely smoothed permittivity exhibited the most similarity with the experimental results, indicating that extremely smoothed permittivity actually mimics complexly intertwined biological tissues. In addition, if the maximum value of the input loss potential is the same as that in the previous paragraph, the maximum value of the transmitted potential and the formed electric field are the same (Figure 3d–f). Although further studies are required to improve experimental measurement methods and tissue mimicry models of real biological tissues to increase the accuracy, the proposed multi-physical simulations can predict the field strength inside biological tissues, which cannot be easily measured. Accordingly, based on the predicted electric field strength by FEA, an optimization study was conducted so that the same output of electric field could appear when the BmET system was applied to in vitro setup. Through the optimization study, tried to unravel the missing link between the ex vivo and in vitro experiments of the BmET-based ES system.

2.3. Unraveling the Missing Link toward Cell Electrical Stimulation

For the in vitro setup, the semi-capacitive coupling (semi-CC) structure proposed in our previous studies[2a,b] was used to mimic the structure of the BmET-based ES (**Figure 4**a and Figure S8, Supporting Information). Based on the semi-CC in vitro setup and to reduce the complexity of the FEA, a 2D axisymmetric-based multi-physical analysis was first conducted (Figure 4b). The circuit model was implemented in FEA similar to ex vivo simulation and cell culture media with a relative permittivity of

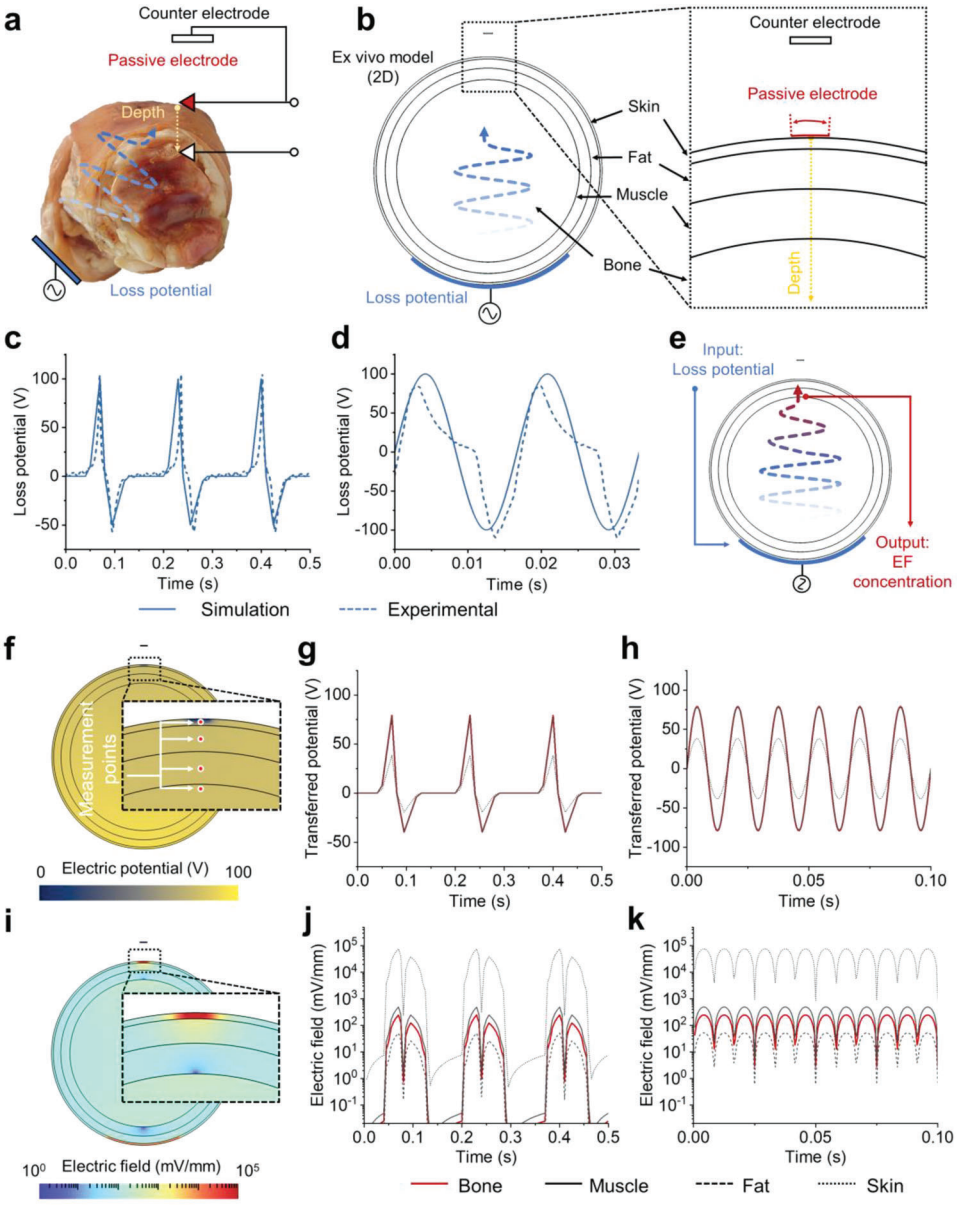

Figure 2. Interrelationship between the experimental measurement and simulation analysis of the ex vivo setup. a) Ex vivo setup for measuring the electric field in biological tissues. The pork front foot consisting of bone, muscle, fat, and skin. b) Ex vivo model for 2D multi-physical simulation. 2D ex vivo model consisting of bone, muscle, fat, and skin (with radii of 45, 47.5, 49.5, and 50 mm, respectively). c) Non-sinusoidal loss potential input from physical activity. d) Sinusoidal loss potential input. e) Input (loss potential) and output (electric field concentration) of 2D multi-physical simulation. f) Electric potential distribution via BmET and circuit model. g) Transferred potential in biological tissues via non-sinusoidal loss potential. h) Transferred potential in biological tissues via sinusoidal loss potential. i) Electric field distribution via BmET and circuit model. j) Strength of electric field in biological tissues via non-sinusoidal loss potential. k) Strength of electric field in biological tissues via sinusoidal loss potential.

50 was used. Subsequently, the electric fields were analyzed according to the horizontal and vertical directions from the center of the dish (Figure 4c). To achieve the electric field intensity calculated in the ex vivo results, the magnitude of the input loss potential was adjusted to 20 V (Figure 4d). Similar to the ex vivo model, the attached input electrode on the outer bottom of the cell culture plate exhibited a large area. As the distance from the input electrode increased, the strength of the electric field gradually increased (Figure 4e). This distribution of the electric field is because the area where the electric field is formed decreases as it approaches the passive electrode and the electric flux density increases. As osteoblast cells are generally located on the outer part of the bone (within ≈0.1 mm), the loss potential input was observed to exhibit similar electric field strength as that of the outer part of the bone, which was calculated in the ex vivo model.[10] Consequently, it was concluded to apply an external loss potential (20 V) for an optimized electrical input for cell stimulation with similar electric field output (≈10^2 to 10^3 mV mm^{-1}) of the

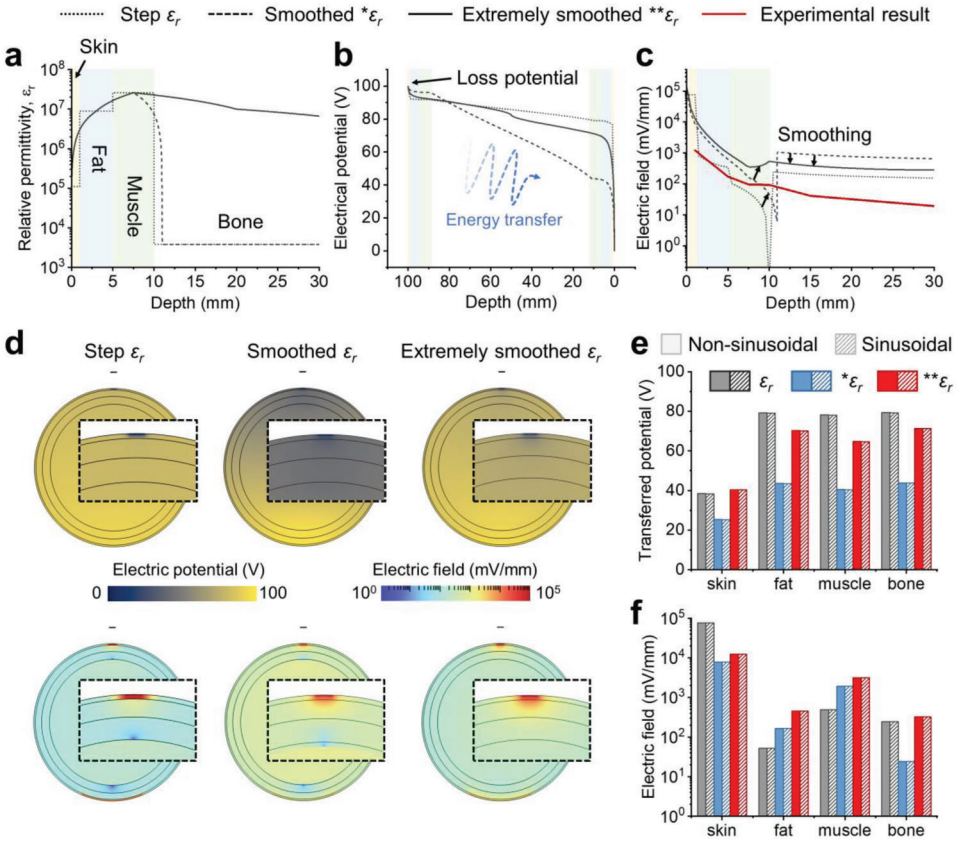

Figure 3. 2D ex vivo simulation using revised permittivity for real biological tissues. a) Relative permittivity distribution in biological tissues. b) Electrical potential distribution in biological tissues according to the revised permittivity model. c) Electric field distribution in biological tissues according to the revised permittivity model. d) Images of the electrical potential and electric field distributions via BmET. e) Transferred potential in biological tissues according to the revised permittivity model and types of loss potential. f) Electric field in biological tissues according to the revised permittivity model and types of loss potential.

ex vivo model. Therefore, the 20 V of loss potential input was selected to investigate the enhanced cellular functions upon the electrical stimulation.

2.4. Accelerated Osteogenic Differentiation by BmET-Based ES

To determine the effect of the BmET-based ES, an in vitro model was implemented using osteogenic cells which are a cell model that could investigate the effect of cell electrical stimulation most accurately and clearly. In this study, the MC3T3-E1 cell, which is a mouse pre-osteoblast cell widely used for investigating osteoblast differentiation, was used for the in vitro experiments. Before examining the various cellular functions, a LIVE/DEAD assay was performed to evaluate the cytotoxicity of the ES. From days 1 to 7, electrically stimulated groups (ES group) and unstimulated groups (CTRL group) were stained with two different fluorescent dyes used to label live and dead cells (**Figure 5**a) and there was no cytotoxicity in the ES group for the entire stimulation period. Subsequently, the cell proliferation behavior of the CTRL group and ES group was compared (Figure 5b). On day 1, there was no significant difference between the CTRL and ES groups. In contrast, on day 4, the cell viability of the ES group was ≈1.3 folds higher than that of the CTRL group, indicating that the ES group exhibited an increased proliferation rate. However, it seems that the MC3T3-E1 cells reached a cell proliferation stagnation phase on day 7, suggesting that the cells entered the verge of osteogenic differentiation. The LIVE/DEAD and increased cell proliferation data by ES demonstrated the non-cytotoxicity of BmET-based ES and optimized ES for cell stimulation, which appears to unravel the missing link between ex vivo and in vitro.

Further in vitro experiment was conducted to verify whether the application of the electrical output from BmET to the pre-osteoblasts accelerated the osteogenic differentiation. For the brief mechanisms of the elect-activation of cells (Figure 5c), the cells have a property for maintaining their membrane potential, of which the potential difference across the plasma membrane was approximately −49.6 mV, and the potential is called resting potential.[11] When the resting potential is changed by external stimulation, the cells try to recover the changed potential into resting potential for cell homeostasis and the depolarization of cells is occurred. At this time, the cells control the various ion channels in the cell membrane to regulate the flux of ions such as Ca^{2+}, K^+, Na^+, or Cl^- to recover resting potential. Therefore, depolarization could increase ion acceptance to recover the membrane potentials.[12] The increased ion acceptance not only regulates the cell membrane potential but also accelerates the synthesis of such various growth factors (e.g., BMP-2), adenosine

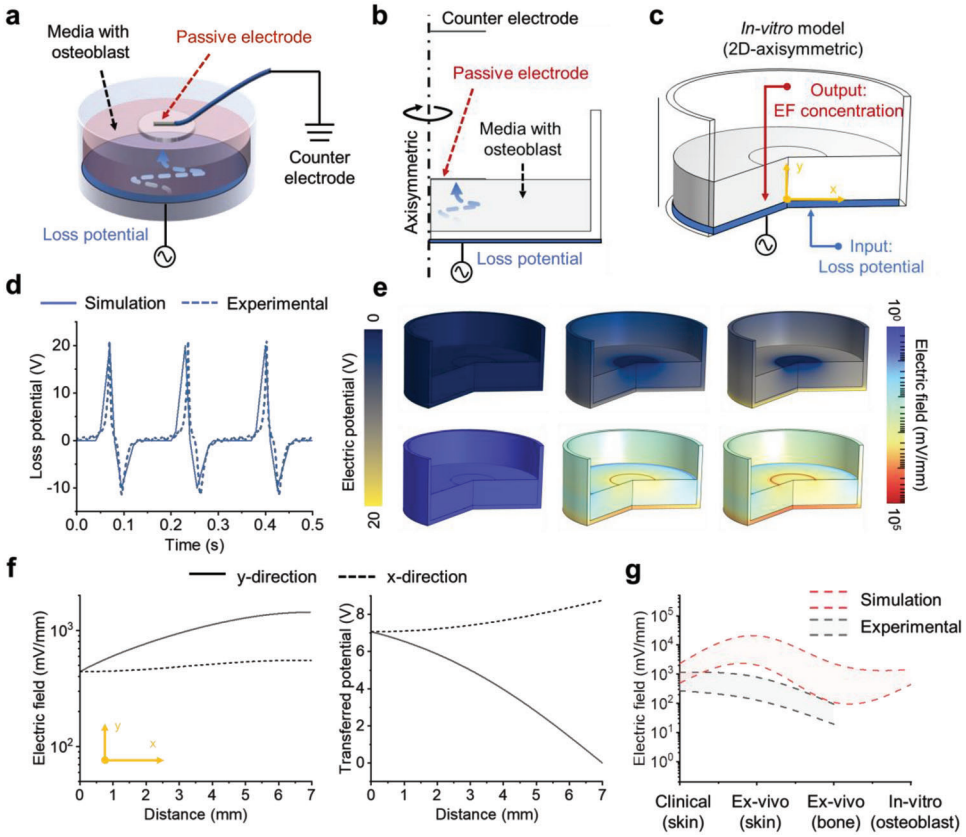

Figure 4. Unraveling the missing link between ex vivo and in vitro setups. a) semi-CC structure for mimicking the BmET-based ES. b) 2D axisymmetric model of the in vitro setup. Electrical potential distribution in biological tissues according to the revised permittivity model. c) Input (loss potential) and output (electric field concentration) of the 2D axisymmetric and multi-physical simulation. d) Loss potential input (20 V) adjusted for obtaining a similar electric field intensity to the ex vivo results. e) Electrical potential and electric field distribution in the 2D axisymmetric model of the in vitro setup. f) Electric field and electrical potential according to the horizontal and vertical directions from the center of the dish. g) Electric field measured and calculated in various setups.

triphosphate (ATP), or extracellular matrix (e.g., collagen). Therefore, cellular functions such as cell proliferation and migration could be increased by the above process. So, when the ES was applied to the cells, the cell membrane potential was changed, the imbalance of the membrane potential altered the transmembrane potential, and depolarization occurred. The depolarization causes the elect-activation of ion channels called voltage-gated ion channels (VGICs), such as Ca^{2+} ion channels, which induced the influx of Ca^{2+} ions toward the cytoplasm.[12,13] At this stage, inorganic phosphate (Pi) also can be transported into the cytoplasm via type III sodium-phosphate cotransporter (NPT3).[14] Subsequently, the introduced calcium ions and Pi into the cytoplasm stimulated the signaling pathways involved in osteogenesis, resulting in the increased synthesis of collagen, amorphous calcium phosphate (ACP), and hydroxyapatite formation. The osteoblasts could be elect-activated by the overall mechanism, and the accelerated osteogenic differentiation was experimentally confirmed by dividing it into initial stages of differentiation (for 1 week) and maturation stage of differentiation between weeks 3 and 4.[15]

First, the effect on the acceleration of osteogenic differentiation in the initial stages by electrical stimulation was analyzed. Collagen type I (Col I) is one of the main bone extracellular matrix (ECM) components, which is synthesized during proliferation and promotes osteogenic differentiation. Bone morphogenetic protein 2 (BMP-2) is also one of the growth factors related to osteogenic differentiation.[16] In this study, the Col I and BMP-2 secretion of the cells was first measured by performing the enzyme-linked immunosorbent assay (ELISA, Figure 5d). The results revealed that on the 4th day, the amount of Col I secretion in the ES group was ≈1.2 times higher and ≈1.5 times higher on the 7th day than that of the CTRL group. Also, the BMP-2 release showed a similar tendency to Col I release, revealing that it increased 1.24 times on the 4th day and 1.34 times on the 7th day than the CTRL group. This result indicates that the pre-osteoblasts rapidly entered the growth plateau owing to ES, and maximized the synthesis of Col I and BMP-2 to prepare for the initiation of osteogenic differentiation. Next, an alkaline phosphatase (ALP) assay was conducted to analyze the early differentiation behavior of the pre-osteoblasts under the ES (Figure 5e). As expected, the ES group exhibited significantly higher ALP activity than the CTRL group on all days of the assay, and the ALP activity on day 7 was ≈1.6 folds higher in the ES group, indicating the ES elect-activated ALP activity.

The RUNX-2 is a key transcription factor related to osteogenic differentiation and OPN is the structural protein, which

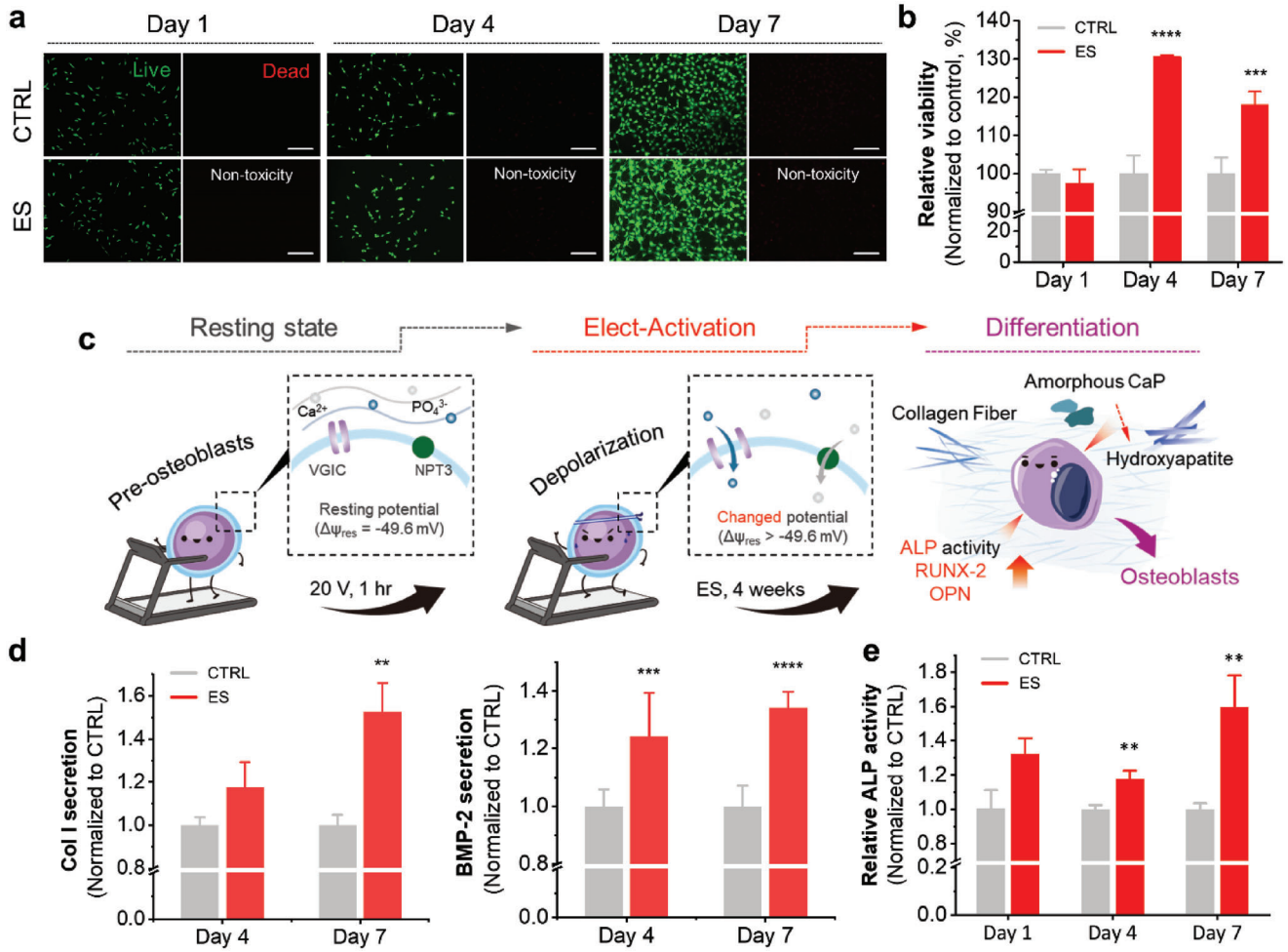

Figure 5. Elect-activation of pre-osteoblasts. a) Live/Dead cytotoxicity assay of the ES of pre-osteoblasts (MC3T3-E1) on days 1, 4, and 7 (scale: 200 μm). b) Increased cell viability ($n = 3$). c) Schematic illustration of the mechanisms of differentiation acceleration of pre-osteoblasts by ES. d) Secretion of collagen type I (Col I, left) and bone morphogenetic protein 2 (BMP-2, right) comparison with CTRL groups ($n = 5$). e) Quantitative analysis of the increased alkaline phosphatase (ALP) activity ($n = 5$). Data are presented as mean ± SD; $*p < 0.05$, $**p < 0.01$, $***p < 0.001$, $****p < 0.0001$ (*t*-test, all experiments were conducted independently).

comprises the mineralized extracellular matrices of bones.[17] These two osteo-specific proteins are significant indicators of osteogenic differentiation, which are expressed during mid-stage of the osteogenesis.[18] In **Figure 6**a, immunofluorescence staining was performed on the 14th day of the ES to compare the respective expression of RUNX-2 and OPN of the ES and CTRL groups. The DAPI indicates the nuclei of the cells. The results revealed that there was a stark contrast in the fluorescence intensity of both markers in the CTRL and ES groups. The quantified intensity of immunofluorescence staining revealed that the expression of both osteo-specific markers was ≈2-fold higher in the ES group compared to the CTRL group (Figure 6b). The overall significant increase in the various cellular activity and osteogenic markers in ES suggests that the BmET-based ES promoted the proliferation and differentiation of pre-osteoblast cells. Subsequently, ARS staining was performed on the 3rd and 4th weeks of the stimulation to evaluate the mineral deposition of the cells (Figure 6c and Figure S9, Supporting Information). This assay could quantitatively analyze the extracellular matrix mineralization, which is the most direct manifestation of osteogenic differentiation.[19] The results revealed that the ES group exhibited significantly higher ARS-stained areas from the 3rd and 4th weeks compared to the CTRL group, indicating that the ES promoted osteogenic differentiation (Figure 6d). Subsequently, protein expressions in ES and CTRL groups were analyzed by liquid chromatography-tandem mass spectrometry (LC-MS/MS) system to verify other proteins affected by BmET-based ES. The volcano plot in Figure 6e shows the proteins up-regulated and down-regulated both in the ES group compared to that in the CTRL group. Surprisingly, it is shown that a large amount of protein was up-regulated by BmET-based ES. The proteins whose expressions were significantly higher in the ES group were classified by their functions in Figure 6e–i. As a result, it was confirmed that proteins involved in protein biosynthesis, protein transport, mitochondrion, and oxidoreductase were up-regulated in the ES group. Especially, proteins related to mitochondrion and oxidoreductase were expressed more than 1.5 folds higher in the ES group (Figure S10, Supporting

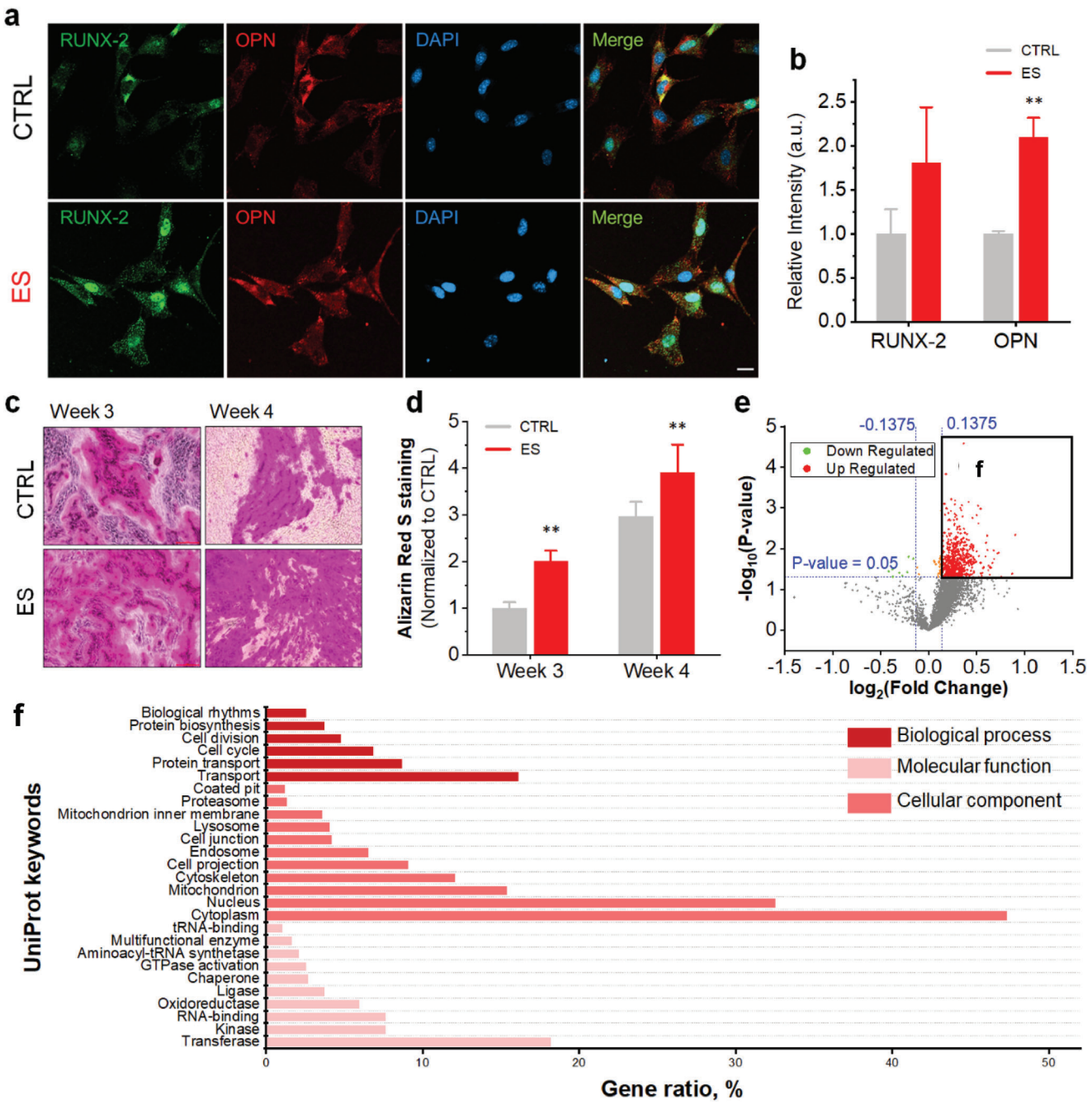

Figure 6. Promoted differentiation by the elect-activation of pre-osteoblasts. a) Immunostaining of the increased expression of RUNX-2 and OPN by ES (scale: 100 μm). b) Quantitative assessment of the RUNX-2 and OPN expression based on the confocal images ($n = 3$). c) Optical microscopy images of the ARS-stained cells. d) Quantitative analysis of the intensity of ARS staining ($n = 5$). e) Volcano plot of the proteins up-regulated and down-regulated in ES compared to CTRL ($n = 3$). Fold change indicates the ratio of the protein intensity in the ES group to that in the CTRL group ($n = 3$). f) Gene annotation performed for the up-regulated proteins in the ES group. Data are presented as mean ± SD; *$p < 0.05$, **$p < 0.01$, ***$p < 0.001$, ****$p < 0.0001$ (*t*-test, all experiments were conducted independently).

Information). It is known that high mitochondrial activity promotes osteogenic differentiation by supplying additional ATP and enhancing the signaling pathway involved in osteogenesis.[20] Also, expression of the proteins related to mitochondrion and oxidoreductase is known to increase as the osteogenic differentiation stage matures.[21] As we already confirmed that the BmET-based ES system stimulates the activity of mitochondria and ATP production,[2b] we concluded that BmET-based ES also stimulates osteogenic differentiation through the activation of mitochondrial functions in addition to the pathway through the induction of calcium ion influx in the cytoplasm and activation of mitochondria.

3. Conclusion

This study addressed two different major subjects: unraveling the missing link of bio-electrical stimulation between ex vivo electrical devices and in vitro bio-electrical stimulations, and the effect of BmET-based ES on cell proliferation and differentiation. To this end, first, a 2D simulation model was constructed based on an ex vivo model, and the consistency of electrical outputs (potential, electric field, waveform) was investigated. Subsequently, the electrical outputs to each tissue (skin, muscle, fat, and bone) were calculated, and compared to the experimental results. The results obtained using the 2D simulation models were perfectly matched with those obtained using the ex vivo models, indicating that a reasonable electric field transmission to bone tissue can be achieved. Using the results, another 2D simulation model based on the BmET-based in vitro setup was constructed and from the electric field calculated using the in vitro model, appropriate electrical input was established. The results revealed that the electrically stimulated cells exhibited increased cellular functions, such as increased proliferation, synthesis of ECMs, and increased differentiations. This study is expected to be able to resolve the suspicious missing link between bio-electrical stimulation and devices, which is currently actively underway.

4. Experimental Section

Materials: Indium tin oxide polyethylene terephthalate (ITO PET; 60 Ω sq^{-1}), alizarin red S (ARS; certificated by the Biological Stain Commission), cetylpyridinium chloride (CPC), and sodium phosphate (Na_3PO_4; 96%) were purchased from Sigma Aldrich Korea. Murine pre-osteoblasts (MC3T3-E1; CRL-2693, subclone 4, ATCC, VA, USA) were used in this study. MC3T3-E1 cells were cultured in a culture flask at 37 °C in a 5% CO_2 incubator. The cell growth media (GM) for MC3T3-E1 cell was prepared using alpha minimum essential medium Eagle (α-MEM, Wellgene) containing 10% fetal bovine serum (FBS, Gibco) and 1% penicillin-streptomycin-glutamine (PS, Gibco). The osteogenic media (OM) was prepared by adding β-glycerophosphate (10 mM), L-ascorbic acid (50 µg mL^{-1}), and dexamethasone (100 nM) to the GM (all osteogenic supplements were purchased from Sigma Aldrich Korea). Trypsin-EDTA (ethylenediaminetetraacetic acid: 0.25%, phenol red) and 1X phosphate-buffered saline (PBS) were purchased from ThermoFisher Scientific (Korea). Mouse-Collagen type I ELISA kit, Mouse BMP-2 ELISA kit, and SensoLyte pNPP alkaline phosphatase assay kit (ALP assay kit, colorimetric) were obtained from Abcam Korea. D-Plus cell counting kit (CCK-8 assay kit) was purchased from Dongin Biotech (Korea). The ALP assay and alizarin red staining was conducted manually, as discussed in the following section.

Experimental Setup for the Measurements of Energy Strength: Since the intensity of the electric field measured on the skin was sensitive to humidity, it was measured in a laboratory where constant temperature (23 °C) and humidity (RH 30%). In the human body, continuous measurement caused sweat and moisture on the skin, and the intensity of the electric field decreased continuously. Therefore, each experiment did not exceed 30 min, and after each experiment, the moisture was removed and dried for more than 5 min before performing the next experiment. In addition, to avoid initial overestimation, the measurement was performed after the electric field strength was stably converged for 5 min. H.Y. performed overall non-invasive measurements of the electric field through the human body.

In ex vivo, to obtain accurate measurements, the electric field intensity was measured in a pork front foot. As blood and juices escape continuously after slaughter, the pork front foot is moister than the general surface of the human body; thus, the pork front foot was dried for at least 24 h before conducting the experiment to avoid underestimation. To transfer the loss potentials to the ex vivo model, input electrodes (5 × 5 cm^2) were employed to ensure sufficient contact with the skin.

Benchtop multimeters and oscilloscopes, which were earth-grounded, overestimated the strength of the potential difference.[22] Therefore, the electric field signal from BmET was measured using signal-grounded hand multimeters (Fluke 289 True-RMS). One terminal of the multimeter was connected to the passive electrode, and the other terminal was connected to a pin-type electrode that was inserted into the biological tissues for accurate measurements. To compare the effects of sinusoidal and non-sinusoidal losses, the root-mean-squared (RMS) values of the voltage and electric field were calculated using the following equations.

$$V_{RMS} = \sqrt{\frac{1}{T}\int [V(t)]^2 dt} \tag{2}$$

$$E_{RMS} = V_{RMS}/x \tag{3}$$

where $V(t)$ is the potential difference over time, T is the total time, and x is the distance between the passive electrode and the measurement electrode (1 mm). The electrical output from the loss potential generators was measured using an oscilloscope (MDO 3014).

Preparation of Potential Generators: To imitate physical activity, a triboelectric generator was fabricated.[23] Polytetrafluoroethylene (PTFE) with a thickness of 0.08 mm (Chukoh Chemical Industries Co,) attached on a circular polymethylmethacrylate (PMMA, diameter of 10 cm) and aluminum (Al) electrode with the same size was utilized as a counter triboelectric material. In addition, a commercial laptop (15ZD960-gx50k, LG notebook) was utilized to generate the sinusoidal loss.

4.0.0.1. Electric Field Simulation: The 2D electric field simulation was analyzed using COMSOL Multiphysics. The connection between the passive electrode and counter electrode was implemented through floating electrode conditions within an AC/DC module. Consequently, the electric potential difference between the electrodes was zero. The loss potential decreased as the distance increased, and as the permittivity of the medium increased, the potential was relatively maintained based on the equation below.

$$-\nabla \cdot (\varepsilon_0 \varepsilon_r \nabla V) = \delta \tag{4}$$

The body-mediated energy transfer and electric field concentration were analyzed in 2D using this governing equation.

Setup for Cell Electrical Stimulation Based on BmET: Cell electrical stimulation (based on the electric field) was performed based on the procedure employed previously by the group.[2a,b] Briefly, prior to cell seeding, the commercial Al-tape was attached to the outer bottom of the cell culture plate (6-well plate) for cell ES. The attached Al-tape was connected to an alternating potential generator, which mimics human movement (charges are induced between the electrodes of the contact layer and transferred to the culture plate, semi-capacitive coupling modality). Subsequently, after seeding the cells in the plates, a custom-made ITO PET electrode for each well was floated on the culture media and connected to a free-charge source. All electrical stimulation experiments of the MC3T3-E1 cell were performed once a day for 1 h (20 V, 6 Hz)

The viability of the MC3T3-E1 cells was assessed using the LIVE/DEAD assay (LIVE/DEAD Cell Viability assay, Invitrogen, NY, USA). The cytoplasm of live cells was stained with calcein AM (green), and the nucleus of dead cells was stained with ethidium homodimer-1 (red). Briefly, 3 × 10^4 cells per well of each cell were seeded in standard 6-well culture plates and cultured under humidified conditions at 37 °C and 5% CO2 for 24 h. Subsequently, the cell culture media was removed from each well, and the cells were washed with 1X PBS. LIVE/DEAD assay reagents were mixed with 10 mL of Dulbecco's phosphate buffered saline (DPBS; Gibco, NY, USA) according to the manufacturer's specifications, after which they were applied to the cells for 40 min at room temperature (RT). Thereafter, the cells were observed using a fluorescence microscope (EVOS FL cell imaging system; Thermo Scientific, Santa Clara, CA, USA).

For the cell proliferation assay, MC3T3-E1 cells were seeded in a 6-well culture plate with a density of 1×10^4 cells per well. Each well was filled with 5 ml GM, which was used as the floating electrode. After electrical stimulation, each well was washed with 1X PBS and 90% (vol%) GM, after which 10% CCK-8 solution was added. After 1.5 h, 200 µL of the media was collected and analyzed using a plate reader ($\lambda = 450$ nm, $n = 5$, SpectraMax 340 PC; Molecular Devices). Cell proliferation assay was conducted on days 4 and 7. Similarly, after conducting electrical stimulation in the same manner, the cell supernatant for each day (days 4 and 7) was collected and the stored samples were analyzed using the collagen type I ELISA kit ($n = 5$).

Analysis of the Enhanced Osteogenic Differentiation by Electrical Stimulation: To induce the osteogenic differentiation of MC3T3-E1 cells, the culture media was changed from GM to OM after the engraftment of the seeded cells. Under the same ES condition, ALP assay was conducted on days 1, 4, and 7 ($n = 5$). Additionally, the cell supernatant for each day (days 4 and 7) was collected and the samples were analyzed using the BMP-2 ELISA kit ($n = 5$). In the case of ARS staining, the staining analysis was conducted after 3 and 4 weeks of ES. After ES, the ARS staining was performed using the following protocol. First, the cells were rinsed with 1X PBS two times, after which they were fixed in an ice-cold 70% ethanol bath for 1 h. Subsequently, the fixed cells were rinsed with deionized water (DW, Human power 1 biotype, Human corporation, 18.3 MΩ) and stained with ARS stock solution (40 mM ARS in DW, pH 4.2, the stock solution was filtrated using a 0.2 µm filter prior to use) for 10 min at RT with gentle agitation. Thereafter, the stained cells were washed using DW five times and with 1X PBS once to remove residual alizarin red stock solution. Lastly, the cells were de-stained with 10% CPC (1 g CPC in 10 mL of 10 mM sodium phosphate, pH 7) for 15 min at RT under gentle agitation, after which 200 µL of the samples were transferred into a 96-well pate and analyzed using a plate reader ($\lambda = 562$ nm, $n = 5$).

Osteogenic differentiation was observed using immunofluorescence staining. Briefly, the MC3T3-E1 cells were seeded on a circular cover glass (Ø 12 mm, Marienfield, Lauda-Königshofen, Germany) at a density of 3×10^3 cells per well in a standard 12-well plate (SPL, Daegu, Korea). The OM was used and replaced every 3 days. After 14 days, osteogenic differentiated cells were fixed with 4% paraformaldehyde phosphate buffer solution (Wako Pure chemical corporation, Osaka, Japan) for 15 min at RT, after which the cells were washed three times with 1X PBS. The cells were permeabilized with 0.1% Triton X-100 in 1X PBS for 10 min at RT and rinsed three times with 1X PBS. The 1% bovine serum albumin solution was treated for 60 min at RT and the cells were incubated with osteopontin (OPN; dilution 1:500, Santa Cruz Biotechnology, CA, USA) and runt-related transcription factor-2 (RUNX-2; dilution 1:400, Cell signaling technology, MA, USA) primary antibody overnight at 4 °C. Highly cross-adsorbed donkey anti-Rabbit IgG, Alexa fluor 488 and donkey anti-mouse IgG, Alexa fluor 555 secondary antibody (dilution 1:400, Thermo Fisher Scientific, MA, USA) were used for staining in the dark for 90 min at RT. The cell nuclei were counter-stained with 4′,6- diamidine-2′-phenylindole dihydrochloride (DAPI; 5 mg mL^{-1}, Invitrogen, NY, USA) for 5 min at RT.

Liquid Chromatography-Tandem Mass Spectrometry (LC-MS/MS)-Based Proteomic Analysis: For proteomic analysis, protein preparation was first performed. Cells from each group were treated with 0.025% trypsin EDTA (ethylene-diamine-tetraacetic acid, ThermoFisher) to detach cells from the culture well. Then, cells were centrifuged at 1500 rpm for 3 min to collect the detached cell pellet. The washing procedure was then performed three times by resuspending the cells in 1X PBS followed by centrifugation and the cell pellet was finally obtained. Then, the cell pellets were homogenized by treating them with 5% SDS (sodium dodecyl sulfate) in 50 mM TEAB (triethylammonium bicarbonate) to extract the proteins from the cells. After heating, alkylation with iodoacetamide, and acidification with phosphoric acid, the binding buffer composed of 90% methanol and 100 mM TEAB was mixed with the protein solution. Finally, the protein solution was loaded onto the filter and centrifuged at 4000× g for 30 s. Then the samples were washed two to three times with a solution of 90:10 methanol:50 mM TEAB and digested with trypsin gold (Promega) at 37 °C overnight at a protein-to-enzyme ratio of 10:1 (w/w). Peptides were eluted stepwise with three elution buffers at a volume of 200 µL each with one more repeat, including 50 mM TEAB in water, 0.2% formic acid in water, and 50% acetonitrile/0.2% formic acid in water. Then, peptides were labeled using a 16-plex TMT reagent (Thermo Scientific, Rockford, IL). Finally, peptides were analyzed by an LC-MS/MS system consisting of an UltiMate 3000 RSLCnano system (Thermo Fisher Scientific) and an Orbitrap Eclipse Tribrid mass spectrometer (Thermo Fisher Scientific) equipped with a nano-electrospray source (EASY-Spray Sources, Thermo Fisher Scientific). Gene annotation of the proteins was performed by DAVID Bioinformatics Resources.

Supporting Information

Supporting Information is available from the Wiley Online Library or from the author.

Acknowledgements

S.J., H.Y., and M.L. contributed equally to this work. This study was supported by the National Research Foundation of Korea (NRF) (No. 2021R1A4A3030268 and 2021R1A2C2091260), the Korea Drug Development Fund funded by the Ministry of Science and ICT, the Ministry of Trade, Industry, and Energy, and the Ministry of Health and Welfare (HN21C1410000021, Republic of Korea), and Korea-England Cooperative Development Program through the National Research Foundation of Korea (NRF) funded by the Ministry of Education (NRF-2021K1A3A1A88100035).

Conflict of Interest

The authors declare no conflict of interest.

Data Availability Statement

The data that support the findings of this study are available from the corresponding author upon reasonable request.

Keywords

bio-electrical stimulations, body-mediated energy transfer, missing-link, triboelectric nanogenerators

Received: March 3, 2023
Revised: May 22, 2023
Published online:

[1] a) M. Kinney, J. Seider, A. F. Beaty, K. Coughlin, M. Dyal, D. Clewley, *Physiother. Theory Pract.* **2020**, *36*, 886; b) H.-J. Yoon, S.-W. Kim, *Joule* **2020**, *4*, 1398.

[2] a) D. Heo, S. Jung, J. Kim, H. Yong, S. Park, D. Kim, S. Cho, K. Cha, H. Ryu, Y. Jin, *Nano Energy* **2022**, *103*, 107772; b) H. Yong, S. Jung, D. Heo, W. Choi, J. Chung, S. Cho, P. Hwang, H. Song, W.-g. Koh, W. Lee, *Nano Energy* **2021**, *87*, 106209; c) M. Verdes, K. Mace, L. Margetts, S. Cartmell, *Curr. Opin. Biotechnol.* **2022**, *75*, 102710; d) Q. Wu, C. Yang, W. Chen, K. Chen, H. j. Chen, F. Liu, D. Liu, H. Lin, X. Xie, W. Chen, *Adv. Sci.* **2022**, *9*, 2202506.

[3] a) M. R. Love, S. Palee, S. C. Chattipakorn, N. Chattipakorn, *J. Cell. Physiol.* **2018**, *233*, 1860; b) R. Luo, J. Dai, J. Zhang, Z. Li, *Adv. Healthcare Mater.* **2021**, *10*, 2100557; c) M. Zhao, H. Bai, E. Wang, J. V. Forrester, C. D. McCaig, *J. Cell Sci.* **2004**, *117*, 397.

[4] J. Zhang, M. Li, E.-T. Kang, K. G. Neoh, *Acta Biomater.* **2016**, *32*, 46.
[5] a) S. Zhang, M. Bick, X. Xiao, G. Chen, A. Nashalian, J. Chen, *Matter* **2021**, *4*, 845; b) Z. Liu, H. Li, B. Shi, Y. Fan, Z. L. Wang, Z. Li, *Adv. Funct. Mater.* **2019**, *29*, 1808820; c) X. Chen, X. Xie, Y. Liu, C. Zhao, M. Wen, Z. Wen, *Adv. Funct. Mater.* **2020**, *30*, 2004673; d) S. Parandeh, N. Etemadi, M. Kharaziha, G. Chen, A. Nashalian, X. Xiao, J. Chen, *Adv. Funct. Mater.* **2021**, *31*, 2105169.
[6] S. Jung, H. Yong, S. Park, D. Kim, S. Ryu, Y.-H. Kim, B. Choi, W. Choi, J.-S. Lee, J. Yoo, *ACS Energy Lett.* **2022**, *7*, 3997.
[7] a) J. Li, Y. Dong, J. H. Park, J. Yoo, *Nat. Electron.* **2021**, *4*, 530; b) S. Maity, M. He, M. Nath, D. Das, B. Chatterjee, S. Sen, *IEEE Trans. Biomed. Eng.* **2019**, *66*, 1791; c) S. Movassaghi, M. Abolhasan, J. Lipman, D. Smith, A. Jamalipour, *IEEE Commun. Surv. Tutorials* **2014**, *16*, 1658; d) J. Park, H. Garudadri, P. P. Mercier, *IEEE Trans. Biomed. Eng.* **2017**, *64*, 452.
[8] H. Yong, D. Heo, B. Kim, H. Moon, K. Choi, D. Kim, S. Lee, *Nano Energy* **2020**, *69*, 104400.
[9] a) S. Gabriel, R. W. Lau, C. Gabriel, *Phys. Med. Biol.* **1996**, *41*, 2251; b) T. Kim, H. Yong, B. Kim, D. Kim, D. Choi, Y. T. Park, S. Lee, *Nat. Commun.* **2018**, *9*, 1437.
[10] a) S. R. Moore, S. Milz, M. L. Knothe Tate, *J Anat* **2014**, *224*, 142; b) O. Duchamp de Lageneste, C. Colnot, in *Periostin* (Ed: A. Kudo), Springer, Singapore **2019**.
[11] a) K. A. DeBruin, W. Krassowska, *Biophys. J.* **1999**, *77*, 1213; b) S. M. Chrysafides, S. Bordes, S. Sharma, **2019**; c) J. A. Fraser, C. L. H. Huang, *J. Physiol.* **2004**, *559*, 459.
[12] a) M. R. Cho, H. S. Thatte, M. T. Silvia, D. E. Golan, *FASEB J.* **1999**, *13*, 677; b) M. R. Cho, J. P. Marler, H. S. Thatte, D. E. Golan, *Front. Biosci.* **2002**, *7*, a1.
[13] a) D. Yamaguchi, J. Green, C. Kleeman, S. Muallem, *J. Biol. Chem.* **1989**, *264*, 197; b) D. Chesnoy-Marchais, J. Fritsch, *J. Physiol.* **1988**, *398*, 291.
[14] S. Sundelacruz, A. T. Moody, M. Levin, D. L. Kaplan, *Bioelectricity* **2019**, *1*, 56.
[15] A. Rutkovskiy, K.-O. Stensløkken, I. J. Vaage, *Med. Sci. Monit. Basic Res.* **2016**, *22*, 95.
[16] R. Baum, E. M. Gravallese, *Clin. Rev. Allergy Immunol.* **2016**, *51*, 1.
[17] T. Komori, *J. Cell. Biochem.* **2011**, *112*, 750.
[18] a) Y. Wei, Y.-H. Chen, L.-Y. Li, J. Lang, S.-P. Yeh, B. Shi, C.-C. Yang, J.-Y. Yang, C.-Y. Lin, C.-C. Lai, *Nat. Cell Biol.* **2011**, *13*, 87; b) J.-M. Kim, Y.-S. Yang, K. H. Park, X. Ge, R. Xu, N. Li, M. Song, H. Chun, S. Bok, J. F. Charles, *Nat. Commun.* **2020**, *11*, 2289; c) E. Kaivosoja, S. Myllymaa, Y. Takakubo, H. Korhonen, K. Myllymaa, Y. T. Konttinen, R. Lappalainen, M. Takagi, *J. Biomater. Appl.* **2013**, *27*, 862.
[19] B. Yu, Z. Qiao, J. Cui, M. Lian, Y. Han, X. Zhang, W. Wang, X. Yu, H. Yu, X. Wang, *Biomaterials* **2021**, *276*, 120997.
[20] a) M. Busch, N. White, L. Shum, R. A. Eliseev, *J. Biol. Chem.* **2018**, *293*, 16019; b) I. K. Kwon, S. C. Lee, Y.-S. Hwang, J. S. Heo, *Biochim. Biophys. Acta, Mol. Cell Res.* **2015**, *1853*, 561.
[21] J. Li, Z. Wang, X. Huang, Z. Wang, Z. Chen, R. Wang, Z. Chen, W. Liu, B. Wu, F. Fang, *Stem Cell Res. Ther.* **2021**, *12*, 1.
[22] a) W. Zhang, G. Gu, H. Qin, S. Li, W. Shang, T. Wang, B. Zhang, P. Cui, J. Guo, F. Yang, G. Cheng, Z. Du, *Nano Energy* **2020**, *77*, 105108; b) G. Shin, H. Yong, J. Chung, E. Cho, J. Ju, Z.-H. Lin, D. Kim, H. Lee, B. Koo, S. Lee, *Nano Energy* **2021**, *82*, 105713; c) J.-S. Lee, H. Yong, Y. I. Choi, J. Ryu, S. Lee, *Int. J. Precis. Eng. Manuf.–Green Technol.* **2022**, *9*, 557.
[23] W.-G. Kim, D.-W. Kim, I.-W. Tcho, J.-K. Kim, M.-S. Kim, Y.-K. Choi, *ACS Nano* **2021**, *15*, 258.